Supplementary Materials for

ACD toxin-produced actin oligomers poison formin-controlled actin polymerization

David B. Heisler, Elena Kudryashova, Dmitry O. Grinevich, Cristian Suarez, Jonathan D. Winkelman, Konstantin G. Birukov, Sainath R. Kotha, Narasimham L. Parinandi, Dimitrios Vavylonis, David R. Kovar, Dmitri S. Kudryashov

correspondence to: kudryashov.1@osu.edu
kudryashova.1@osu.edu

This PDF file includes:

> Materials and Methods
> Figs. S1 to S9
> Table S1
> Captions for Movies S1 to S5

Other Supplementary Materials for this manuscript includes the following:

> Movies S1 to S5
> Modeling Program

Materials and Methods

ACD treatment of IEC-18 cells and cell microscopy. Normal rat intestinal epithelium cells IEC-18 (ATCC CRL-1589) were maintained at a low passage number of 10 to 20 in Dulbecco's modified Eagle's medium (DMEM) with 4 mM L-glutamine, 1.5 g/L sodium bicarbonate, 4.5 g/L glucose, 10% fetal bovine serum in a humidified incubator at 37°C and 5% CO_2. Anthrax toxin delivery machinery (*15-17*) was used for intracellular delivery of ACD toxin. Purification procedures for *B. anthracis* protective antigen (PA) (*18*) and a construct of ACD from *V. cholerae* fused C-terminally to the N-terminal domain of *B. anthracis* lethal factor (LF$_N$), LF$_N$ACD$_{Vc}$ (*17*), for intracellular delivery of ACD were described previously. Catalytically inactive mutant of LF$_N$ACD$_{Vc}$ was generated by mutation of two essential active site glutamate residues to alanines (*19*) (E1990A and E1992A; numbers correspond to amino acid sequence of the full-length MARTX$_{Vc}$ toxin; NCBI accession number AAD21057.1). Purified LF$_N$ACD$_{Vc}$ constructs were mixed with PA at 1:2.5 molar ratios and added to cells at final concentrations of LF$_N$ACD$_{Vc}$ ranging from 0.25 to 1 nM. At the defined time points phase contrast micrograph images of cells were obtained using Nikon inverted microscope Eclipse Ti-E and NIS Elements software (Nikon).

Immunoblotting. Following microscopy, cells were collected and cell lysates were prepared in reducing SDS-PAGE sample buffer. Samples were subjected to PAGE and transferred to nitrocellulose. Membranes were blocked in phosphate buffered saline (PBS, pH 7.4) containing 0.1% Tween-20 and 5% non-fat dry milk for 1 h at room temperature. Primary antibody was added to membranes at various dilutions in the blocking buffer and incubated overnight at 4°C followed by three washes with PBS containing 0.1% Tween-20 and incubation with the corresponding secondary antibody for one hour at room temperature. After final PBS-Tween-20 wash, signal was detected using chemiluminescent HRP substrate WesternBright Sirius (Advansta) in an Omega Lum G imager (Aplegen).

Primary antibody used in this study include anti-actin (ACTN05-C4; 1:2,500 working dilution) and anti-hemagglutinin(HA)-tag (#26183; 1:10,000) from ThermoFisher Scientific; anti-actin (A2228; 1:2,500), anti-FHOD1 (formin homology 2 domain containing 1; SAB1400515; 1:500), and anti-profilin (P0101; 1:500) from Sigma Aldrich; Bethyl Laboratory Inc antibodies (anti-Diaphanous-1 [DIAPH1], A300-077A, 1:10,000; anti-Diaphanous-2 [DIAPH2], A300-079A, 1:10,000; anti-INF2 [inverted formin, FH2 and WH2 domain containing], A303-427A, 1:5,000) and Bioss antibodies (anti-DAAM1 [dishevelled associated activator of morphogenesis 1], bs-4099R, 1:200; anti-FMN2 [formin 2], bs-7748R, 1:250) purchased from One World Lab. Anti-mouse and anti-rabbit secondary antibodies conjugated to HRP (1:10,000) were obtained from Sigma Aldrich.

Transepithelial cell electrical resistance (TEER). Concurrently with the microscopy and immunoblotting procedures described above, TEER was monitored as published previously (*20*). IEC-18 cells were cultured to 90-100% confluence on gold electrodes (Applied Biophysics) at the same passage number and culture conditions as for the microscopy and immunoblotting experiments. The monolayers were then treated with varying concentrations of LF_NACD_{Vc} and PA mixtures as described in the "ACD treatment of IEC-18 cells and cell microscopy" section. TEER was continuously measured on Electric Cell-substrate Impedance Sensing apparatus (ECIS; Applied Biophysics) in a humidified incubator at 37^oC and 5% CO_2 (Fig. 1A). Effects of formin inhibitor SMIFH-2 and Arp2/3 complex inhibitor CK-666 (both obtained from Sigma Aldrich) on IEC-18 epithelial monolayer resistance were assessed by TEER and cell imaging as described above (fig. S3).

Transient transfection and actin-oligomer pull-down (Fig. 1D). Plasmid for mammalian expression of double-tagged actin with N-terminal Twin-Strep-tagII and HA-tag (SHA-actin) was a gift from Dr. Vartiainen (University of Helsinki, Finland). HeLa cells were grown on nine T-75 flasks to 50-70% confluence in complete DMEM medium. Six flasks were transfected with SHA-actin plasmid using

3

Lipofectamine LTX transfection reagent according to the manufacturer instructions (Invitrogen). Following 24 h incubation, transfected cells were treated with mixtures containing PA and either active LF_NACD_{Vc} (added to three transfected flasks) or inactive E1990A/E1992A LF_NACD_{Vc} mutant (added to other three transfected flasks). The remaining three flasks with non-transfected untreated cells were used as a negative control. Final concentrations of PA and LF_NACD_{Vc} were 12.5 and 5 nM, respectively. Cells were incubated for additional 2 h to allow for actin crosslinking by active ACD. Cells from three separate sets of flasks (X: SHA-actin transfected and crosslinked with active LF_NACD_{Vc}; A: SHA-actin transfected, non-crosslinked [treated with inactive LF_NACD_{Vc}]; C: non-transfected, untreated control) were harvested and lysed in 1.5 mL of lysis buffer containing 30 mM Tris-HCl, pH 7.5, 150 mM NaCl, 2 mM DTT, 2 mM $MgCl_2$, 0.5 mM EGTA, 2 mM PMSF, 0.5% nonidet P40, and protease inhibitor cocktail (Sigma Aldrich). Cell lysates were incubated for 15 min at 4°C on a nutator and centrifuged at 10,000 g for 10 min at 4°C. Cleared lysates were combined with Strep-Tactin affinity resin (1.5 mL of lysate per 75 µL of slurry; IBA-Lifesciences) and incubated for 1 h at 4°C rotating. Mixtures were transferred to spin columns and centrifuged at 700 g for 30 sec at 4°C. Following washing with lysis buffer with nonidet P40 reduced to 0.1%, samples were eluted sequentially using lysis buffer without nonidet P40 supplemented either with 0.5 M NaCl or 50% formamide (FA). To detect proteins co-purified with SHA-actin (A) or SHA-actin-oligomers (X), samples were resolved on polyacrylamide gels and subjected to immunoblotting as described above.

Cellular G/F actin assay. To determine whether SHA-tagged actin is able to polymerize normally, we analyzed the relative proportions of G- and F-actin in SHA-actin transfected HeLa cells (fig. S2A,B). Briefly, cells from 35 mm plates were lysed in 60 µl of F-actin stabilization buffer (50 mM PIPES, pH 6.8, 50 mM NaCl, 5 mM $MgCl_2$, 5 mM EGTA, 5% glycerol, 0.1% TritonX-100, 0.1% Nonidet P-40, 0.1% Tween-20, 10 mM β-mercaptoethanol, protease inhibitor cocktail), passed through 29-gauge needle, and incubated on ice for 10 min. Cell lysates were cleared from debris by centrifugation at 350 g for 5 min.

Following ultracentrifugation at 300,000 g for 30 min using TLA-100 rotor in Optima TL-100 ultracentrifuge (Beckman Coulter), supernatants (containing G-actin) were collected and supplemented with reducing SDS-PAGE sample buffer. The pellets (containing F-actin) were soaked in the initial volume (60 μl) of F-actin stabilization buffer supplemented with reducing SDS-PAGE sample buffer. After 1 h incubation on ice, pellets were resuspended by vigorous pipetting. All samples were boiled for 2 min; 20 μl fractions were subjected to anti-actin immunoblotting.

Immunofluorescence. To further verify that SHA-tagged actin can polymerize into F-actin structures, 3T3 mouse fibroblasts were grown on 8-well μ-slides (Ibidi), transfected with SHA-actin plasmid using Lipofectamine LTX transfection reagent (Invitrogen), and incubated for 24 h. Transfected cells were fixed in 2% paraformaldehyde in PBS, permeabilized with 0.2% Triton X-100 in PBS, blocked with 1% BSA in PBS, and stained with anti-HA antibody (1:1,000 final dilution) followed by anti-mouse-TRITC antibody (Sigma Aldrich). Cells were then counterstained with FITC-phalloidin (Cytoskeleton) and Hoechst dye (Life Technologies), mounted in Ibidi mounting medium, and visualized by fluorescence microscopy using Nikon inverted microscope Eclipse Ti-E (fig. S2C).

Protein purification.

A. Actin was prepared from acetone powder of rabbit skeletal muscle (Pel-Freeze Biologicals) as previously described (_21_), gel filtered, stored on ice in G-buffer (5 mM Tris-HCl, pH 8.0, 0.2 mM CaCl$_2$, 0.2 mM ATP, 5 mM β-mercaptoethanol [βME]) and used within 2 weeks. Pyrene, Oregon Green, and tetramethylrhodamine (TMR) labeled actins were prepared as previously described (_22_).

B. ACD-crosslinked actin oligomers were prepared using thermo-labile ACD from _Aeromonas hydrophila_ (ACD$_{Ah}$) (_23_). Both ACD$_{Vc}$ and ACD$_{Ah}$ produce actin oligomers with similar efficiency, yield, composition, SDS-gel mobility, and with a similar pattern of formin inhibition. For all in vitro experiments, we selected to use ACD$_{Ah}$ as a thermo-labile isoform of the enzyme, which, in contrast to ACD$_{Vc}$, can be

5

completely inactivated under mild heating conditions (*23*), which are well tolerated by actin oligomers (fig. S5C). This selection was critical to allow quantitative analysis and to ensure that no additional actin oligomers were produced from the monomeric actin (present in all the polymerization assays) due to incomplete inhibition or incomplete removal of the toxin. To prepare ACD-free actin oligomers, G-actin was diluted to 20 μM in reaction buffer (5 mM Tris-HCl, pH 8.0, 0.2 mM ATP, 0.1 mM phenylmethanesulfonylfluoride [PMSF]), mixed with 10 nM ACD_{Ah}, (2000:1 mole ratio of actin to ACD), and 1 mM $MgCl_2$ was added to initiate crosslinking. The crosslinking reaction of monomeric G-actin into non-polymerizable actin oligomers was allowed to proceed for 25 min at 10^oC and terminated by heat-inactivation of ACD_{Ah} at 42^oC for 20 min (fig. S5B,C). These conditions favor actin crosslinking versus actin polymerization – two reactions, which compete with each other. To remove the leftover uncrosslinked actin, the concentration of $MgCl_2$ was brought to 3 mM and the sample was incubated at 25^oC for 30 min to ensure complete polymerization of all uncrosslinked actin, which was then removed by centrifugation at 300,000 g for 30 min at 4^oC using a TLA-100 rotor in an Optima TL-100 ultracentrifuge (Beckman Coulter). The supernatant fraction, containing non-polymerizable actin oligomers, was supplemented with 1 mM ATP, stored on ice, and used within seven days. Because of the heterogeneity of actin oligomer species (i.e. simultaneous presence of dimers, trimers, tetramers, and higher order species; fig. S5B), it was impossible to correctly express their molar concentration. Therefore, oligomer concentrations were determined by Bradford assay (Bio-Rad) using monomeric actin of known concentration as a standard, without correcting for the difference in sizes between actin and the oligomers. Therefore, the actual molar concentration of oligomeric species was smaller than indicated. Actin dimers (fig. S5B) were prepared as described previously (*24*) except that ACD_{Ah} was used and inactivated at 42^oC as described above.

C. Human profilin 1 (PNF1) was expressed in BL21(DE3)pLysS *E. coli* using rich bacterial cell growth medium (1.25% tryptone, 2.5% yeast extract, 125 mM NaCl, 0.4% glycerol, 50 mM Tris-HCl, pH

8.2) and purified on poly-L-proline sepharose resin as previously described (*25*). Purified profilin was dialyzed against three buffer changes of profilin storage buffer (2 mM Tris-HCl, pH 8.0, 0.2 mM ethylene glycol tetraacetic acid [EGTA], 1 mM DTT, 0.1 mM PMSF).

D. Formins were prepared as follows: mouse formin mDia1(14PP), a construct containing FH1, FH2 and DAD domains (residues 552-1255 including all 14 poly-proline stretches of FH1 domain (*11*); mDia1 NCBI accession number NP_031884.1) in a pET21a vector with N-terminal maltose binding protein (MBP) and C-terminal 6xHis tags (fig. S5A,B), was prepared as described previously (*26*). FH1-truncated mutants mDia1(5PP) (residues 671-1255 with 5 poly-proline repeats in FH1 domain), mDia1(2PP) (residues 717-1255 with 2 poly-proline repeats), and mDia1(FH2) (residues 739-1255 without any poly-proline repeats) were generated from MBP-mDia1(14PP)-6xHis template using the In-Fusion Mutagenesis Cloning protocol (Clontech). All constructs were expressed in *E. coli* BL21-Gold (DE3)pLysS (Aligent Technologies) in a rich bacterial cell growth medium supplemented with 1 mM L-proline to boost the translation of poly-proline-rich regions. Expression was induced by the addition of 1 mM IPTG and cells were allowed to grow for 20 h at 16°C. All constructs were purified using Talon metal affinity resin (Clontech), eluted with buffer containing 50 mM sodium phosphate, pH 8.0, 0.5 M NaCl, 10% glycerol, 2.5 mM βME, 0.5 mM PMSF, 250 mM imidazole, and dialyzed against formin storage buffer (20 mM Tris-HCl, pH 8.5, 50 mM NaCl, 5% glycerol, 1 mM DTT, 0.1 PMSF). Purification of SNAP-tagged mDia2 and labeling it with SNAP-Surface 549 (New England Biolabs) were conducted as described (*27*). All formins were kept on ice or stored at -20°C in the storage buffer with 50% glycerol.

Total internal reflection fluorescence microscopy (TIRFM) (Fig. 2, 3; fig. S4). TIRF microscopy experiments were performed as described previously (*10*). Briefly, rabbit skeletal actin (33% labeled Oregon Green actin or 15% TMR-actin; 1.5 μM final concentration) was switched from Ca^{2+}- to Mg^{2+}-ATP state by incubation with exchange buffer (final composition: 50 μM $MgCl_2$, 0.2 mM EGTA) for 2

min. Actin was added to the mixture of an mDia1 formin construct (either 14PP, 5PP, 2PP, or FH2; 5 nM final concentration) with or without PFN1 (0 or 2.5 µM final concentration) and varying concentrations of ACD_{Ah}-crosslinked actin oligomers in the following final buffer composition: 10 mM imidazole, pH 7.0, 110 mM KCl, 50 mM DTT, 1 mM $MgCl_2$, 1 mM EGTA, 0.2 mM ATP, 50 µM $CaCl_2$, 15 mM glucose, 20 µg/mL catalase, 100 µg/mL glucose oxidase, 3% glycerol, and 0.5% methylcellulose-400cP (Sigma Aldrich). Immediately after adding actin, samples were transferred to a NEM-myosin treated flow chamber (*28*). For most of the TIRFM experiments, images were collected with an iXon EMCCD camera (Andor Technology) using an Olympus IX-71 microscope fit with through-the-objective TIRF illumination. For two-color TIRF experiments (Fig. 2E), 1.5 µM TMR-actin, 5 nM mDia1(14PP), and 2.5 µM PFN1 were polymerized for 200 s in a flow chamber, and then the flow chamber solution was replaced with 1.5 µM Oregon Green actin, 20 nM actin oligomers, and 2.5 µM PFN1. Filaments were manually tracked and measured using ImageJ software (*29*). Additionally, polymerization of 1.5 µM Oregon Green actin in the presence of 1 nM SNAP-Surface-549-mDia2 and 2.5 µM PFN1 (Fig. 3A) was monitored in the presence or absence of 20 nM actin oligomers on PEG-Si treated glass chamber (*30*).

The oligomer-induced inhibition of nucleation by mDia1(FH2) (fig. S4D-G) was assessed using Nikon Eclipse Ti-E microscope equipped with a perfect focus system, through-the-objective TIRF illumination system, and DS-QiMc camera (Nikon). The effects of the oligomers on filament nucleation were assessed by pre-mixing Mg^{2+}-Oregon Green actin (33% labeled) and actin oligomers in the presence or absence of PFN1. This mixture was added to the reaction containing mDia1(FH2) to result in the final concentrations of 1.5 µM Oregon Green actin, 1 nM mDia1(FH2), 100 nM of actin oligomers in the absence of PFN1 (fig. S4D,E) or 10 nM of mDia1(FH2) formin, 150 nM of actin oligomers in the presence of 2.5 µM of PFN1 (fig. S4F,G). In both cases the concentrations of the oligomers were selected to cause

83-86% of inhibition as based on the IC_{50} values obtained from bulk actin polymerization assays (Fig. 4E, F). Filaments were counted at the 180-second interval in each case.

Pyrenyl-actin polymerization assays (Fig. 4A-G; fig. S5F-H, S6, S7). Gel-filtered Ca^{2+}-ATP G-actin (5% pyrenyl-labeled; 2.5 µM final concentration, unless otherwise noted) were pre-mixed in black 384-well plates with 10 nM of mDia1 formin constructs, 5 µM PFN1, and varying (0-500 nM) concentrations of actin oligomers (all concentrations are given as final) in the reaction buffer (10 mM MOPS, pH 7.0, 0.2 mM ATP, 0.5 mM DTT). Then, Ca^{2+}-ATP G-actin was converted to Mg^{2+}-ATP actin by adding 0.066 volumes of switch buffer (150 mM MOPS, pH 7.0, 3 mM ATP, 7.5 mM DTT, 4.5 mM EGTA, 1.5 mM $MgCl_2$) and incubating at room temperature for 1 min. Polymerization was initiated by adding 0.33 volumes of initiation buffer (30 mM MOPS, pH 7.0, 0.6 mM ATP, 1.5 mM DTT, 3 mM $MgCl_2$, 150 mM KCl). Pyrene fluorescence was monitored at λ_{ex} = 365 nm and λ_{em} = 407 nm using an Infinite M1000 Pro plate reader (Tecan). Inhibition of polymerization by actin oligomers (Fig. 4E,F) was assessed by calculating the tangent slope of each pyrene fluorescence trace at 50% (40-60% interval) of maximum polymerization and fitting the obtained data to a binding isotherm equation as previously described (*31*) using Origin software (OriginLab):

$$\frac{\Delta F}{\Delta F_{max}} = \frac{M+X+IC_{50}-\sqrt{(M+X+IC_{50})^2-4\cdot M\cdot X}}{2\cdot M},$$

where M – mDia1 formin concentration, X – concentration of crosslinked actin oligomers, and IC_{50} – the oligomer concentration causing 50% inhibition of the formin activity. ΔF – the observed pyrene fluorescence change. ΔF_{max} – the maximum pyrene fluorescence change.

To determine the apparent inhibition constant ($_{app}K_i$) of mDia1(14PP) formin by the oligomers (Fig. 4G), IC_{50} values were calculated as above for two actin concentrations: 1 and 2.5 µM. The obtained IC_{50} values were then used in the Cheng-Prusoff equation (*32*):

9

$$appK_i = IC_{50}/(1 + A/appK_d),$$

where A – actin concentration and $_{app}K_d$ – an apparent dissociation constant of actin for formin.

Effects of the oligomers on mDia1-controlled filament nucleation were evaluated by seeding assays conducted in the absence and presence of PFN1 (fig. S7). For seeds generated in the absence of PFN1 (fig. S7A-F), polymerization of 2.5 µM of unlabeled actin in the presence of 10 nM mDia1(14PP) or mDia1(FH2), and with or without 100 nM of actin oligomers was initiated as in standard pyrene assay (see above). After 90 s of polymerization (when less than 30% of total actin is expected to be polymerized), an aliquot was extracted and diluted in the initiation buffer. The resulted mixture was immediately used to initiate polymerization of 1.0 µM pyrene actin (5% labeled) in the absence (fig. S7A,C) or presence of 5 µM PFN1(fig. S7B,D) to yield a 100-fold final dilution of the original seeds and to ensure that the final concentration of the oligomers (1 nM) is sufficiently low to not substantially affect the filament elongation rate. For seeds generated in the presence of PFN1 (5 µM; fig. S7G,H), only mDia1(FH2) was used to avoid misinterpretation of the results due to the high affinity of the oligomers to mDia1(14PP)-FH1 domains and their strong influence on the filament elongation rate. The experiments were conducted similarly to those in the absence of PFN1, except that seeds were allowed to grow for 300 s before using them in the pyrene assay.

Statistical analysis. Data were analyzed using Microsoft Excel (Microsoft Corporation), Origin (OriginLab), and KaleidaGraph (Synergy Software). Errors represent standard errors of mean values (SEM). Statistical significance was determined by two-tailed Student's t-test ($p<0.05$).

Modeling of actin filament nucleation and elongation in the presence of actin oligomers. We developed an ordinary differential equations model to describe the polymerized actin fraction as a function of time (see Supplementary Modeling Program), based on prior modeling work (*11, 33, 34*).

A. Mechanisms included in the model:

(1) Binding of profilin to actin. We assume that unpolymerized ATP-actin monomers (total concentration A_{unpol}) are in a binding equilibrium with profilin of total concentration P_{tot} such that the concentrations of free ATP-actin, A, and profilin-actin, PA, are given by:

$$A = 0.5\left(A_{\text{unpol}} - P_{\text{tot}} - K_{PA}^{d}\right) + 0.5\sqrt{\left(P_{\text{tot}} - A_{\text{unpol}} + K_{PA}^{d}\right)^{2} + 4A_{\text{unpol}}K_{PA}^{d}}, \tag{1}$$

$$PA = A_{\text{unpol}} - A, \tag{2}$$

where K_{PA}^{d} is the profilin-actin dissociation constant.

(2) Filament elongation. Oligomers bind to formin-associated filaments transiently, interrupting periods of growth by pauses. Thus, we assume that the elongation rate of oligomer-free filaments is the same function of total actin and profilin as in the absence of oligomers, $j_F(A_{\text{unpol}}, P_{\text{tot}})$. Previous models of formin-associated elongation have studied the dependence of j_F on the rates of processes such as binding of profilin and profilin-actin to regions of the FH1 domain and transfer of profilin-actin to the barbed end (*11, 34, 35*). Fitting of such models to experimental data depends on assumptions about the role of ATP hydrolysis in the formin-mediated polymerization cycle (*11, 12, 34, 36*). Since our emphasis here is on the role of oligomers, instead of implementing a detailed model of the formin polymerization cycle, we postulate an empirical functional form for $j_F(A_{\text{unpol}}, P_{\text{tot}})$ that matches the dependence seen in prior experimental data with mDia1 (*10*) and also gives a formin-mediated elongation rate of 32 sub/sec at the concentration conditions corresponding to fig. S4A (see fig. S8A):

$$j_F(A_{\text{unpol}}, P_{\text{tot}}) = A_{\text{unpol}}\left(3\,\mu\text{M}^{-1} + 7\,\mu\text{M}^{-1}e^{-P_{\text{tot}}/(1.5\mu M)} + 17\,\mu\text{M}^{-1}r_{\text{PP}}P_{\text{tot}}e^{-[P_{\text{tot}}/(3\mu M)]^{0.65}}\right). \tag{3}$$

Here parameter r_{PP} represents the reduction of FH1-mediated polymerization in formin constructs with truncated FH1 domains, being 1 for full-length FH1-FH2 mDia1 and 0 for FH2 only. Reduction of the value of parameter r_{PP} reproduces the effect of reduction of elongation rate with reduction in the number

of poly-proline FH1 domains (*11, 34, 35, 37*) (fig. S8A). Since the largest concentration of profilin in the bulk polymerization experiments of this work is 5 μM, the precise functional dependence of j_F at higher profilin concentrations is of no consequence to the following.

We model formin-free actin filament elongation by two rate constants, k_A^+ and k_{PA}^+, that describe the association of actin and profilin-actin to the barbed end, respectively. We neglect the pointed end and actin filament depolymerization, which depends on assumptions about the role of profilin in the critical concentration of ATP-actin (*38*). Thus we do not account for the final presence of ~ 0.1 μM of unpolymerized actin out of the total A_{tot} = 2.5 μM used in experiments in the absence of profilin. In the presence of profilin, a higher fraction of actin may remain unpolymerized, up to A_{unpol} = 0.73 μM, if K_{PA}^d = 0.7 μM (*39-42*) and A_{free} = 0.1 μM at long times.

(3) Binding of oligomers to formins. Free oligomers in the solution are assumed to bind to and dissociate from formin-associated filaments with rates $k_{on} O_{free}$ and k_{off}, respectively, where O_{free} is the concentration of free oligomers in the bulk. The association of oligomers with free formin dimers, leading to assumed inhibition of formin-mediated nucleation, is modeled as an equilibrium second-order reaction with dissociation constant $K_{OF_{free}}^d$:

$$O_{free} = 0.5\left(O_{bulk} - F_{bulk} - K_{OF_{free}}^d\right) + 0.5\sqrt{\left(F_{bulk} - O_{bulk} + K_{OF_{free}}^d\right)^2 + 4O_{bulk}K_{OF_{free}}^d}, \tag{4}$$

where F_{bulk} is the concentration of formin dimers that are not associated with filaments (we assume all formins form dimers) and O_{bulk} is the concentration of oligomers not bound to filaments. Denoting *BF* and *BFO* the concentrations of formin-associated and formin-oligomer-associated barbed ends, mass conservation implies:

$$O_{bulk} = O_{tot} - O_{pol} - BFO, \quad F_{bulk} = F_{tot} - BF - BFO, \quad F_{free} = F_{tot} - BF - BFO - (O_{bulk} - O_{free}), \tag{5}$$

where F_{free} is the concentration of free formin dimers and O_{pol} is the concentration of polymerized oligomers (see item 5 below).

(4) *Actin filament nucleation.* Since the main pathway for nucleation involves the formation of a trimer (*43*), which could incorporate a profilin at one of its subunits, we use a rate constant k_A^{nuc} to describe the rate of filament formation (*33, 34*). In the presence of formins, we assume the nucleus is a formin dimer bound to two free actin subunits or one free and one profilin-actin. Since the latter rate may be assisted by the presence of the FH1 domain, this gives two more nucleation rate constants, k_{AF}^{nuc} and k_{APF}^{nuc}. The nucleation parameters are determined by fitting the model results in the absence of oligomers to experiments with actin, profilin + actin, actin + formins, and actin + formins + profilin. The resulting values are found to be of the same order of magnitude as those reported in prior works (*33, 34*) (see Table S1).

(5) *Incorporation of oligomers into filaments, oligomer-induced severing, and spontaneous fragmentation.* Oligomers are assumed to polymerize at formin-free filaments with rate constant k_O^+. Polymerized oligomers induce severing, resulting in the formation of a new barbed end, with rate constant k_O^{sev}. Including this reaction leads to better fits to the experimental curves in the absence of profilin, depending on the value of the product $k_O^+ k_O^{\text{sev}}$. Spontaneous filament fragmentation with rate k^{frag} of order the value estimated in prior works (*44, 45*), improves the fits to the data at long times so it is included in the model (however the main conclusions are not significantly influenced by spontaneous fragmentation).

B. Rate Equations:

The following equations describe the evolution of concentrations over time, with the free barbed end concentration denoted by B:

$$\frac{dA_{\text{unpol}}}{dt} = -k_A^+ B \cdot A - k_{PA}^+ B \cdot PA - j_F(A_{\text{unpol}}, P_{\text{tot}}) \cdot BF - 3k_A^{\text{nuc}}(A^3 + A^2 \cdot PA) - 2k_{AF}^{nuc} A^2 F - 2k_{APF}^{nuc} A \cdot PA \cdot F \quad (6)$$

$$\frac{dB}{dt} = k_A^{nuc}(A^3 + A^2 \cdot PA) + k_O^{sev}O_{pol} + k^{frag}(A_{tot} - A_{unpol}) \tag{7}$$

$$\frac{dBF}{dt} = k_{AF}^{nuc}A^2 \cdot F + k_{APF}^{nuc}A \cdot PA \cdot F + k_{off}BFO - k_{on}O_{free} \cdot BF \tag{8}$$

$$\frac{dBFO}{dt} = -k_{off}BFO + k_{on}O_{free} \cdot BF \tag{9}$$

$$\frac{dO_{pol}}{dt} = k_O^{+}B \cdot O_{free} \tag{10}$$

Equations (1)-(10) define the evolution of the system in time, given appropriate initial conditions. The parameter values used are shown in Table S1. The equations were integrated numerically and the accuracy of the solution was checked using several numerical integration methods. The results in fig. S8 that report the polymerized fraction, $(A_{tot} - A_{unpol})/A_{tot}$, versus time use the Euler-Richardson scheme with a time step 0.5 sec or smaller.

C. Model Results:

We first checked that the model reproduces the experimental observations in Fig. 4B, after adjusting the values for spontaneous nucleation, k_C^{nuc}, and fragmentation, k^{frag} (fig. S8B). Addition of oligomer incorporation and oligomer-induced severing in the model increases the slope of the actin alone polymerization curve at the late stages of polymerization but does not significantly modify it at short times (fig. S8C). The model accurately reproduces the polymerization kinetics only if the parameters describing oligomer incorporation and oligomer-induced severing are smaller in the presence of profilin as compared to the case of pure actin (fig. S8B,C), consistent with Fig. 4A,B. In the following we assume that oligomers do not incorporate efficiently into filaments in the presence of 5 μM profilin in accordance with our experimental data (fig. S5D). We note that the model parameters are slightly adjusted for each panel in fig. S8 to account for the variability of the control polymerization curves in each set of experiments.

We then fitted the model to polymerization curves in the presence of mDia1(14PP), with and without profilin, as in Fig. 4C,D but without oligomers. Fits to those curves allowed us to estimate the two parameters describing formin-mediated nucleation kinetics, k_{CF}^{nuc} and k_{CPF}^{nuc} (fig. S8D,E). Since the kinetics of oligomer binding to a formin-associated barbed end can be directly measured from experiments with TIRFM, this leaves the dissociation constant of oligomers bound to free formins as the only unconstrained parameter to fit the polymerization curves in the presence of oligomers. In the presence of profilin, k_{on} and k_{off} were directly measured in Fig. 3. In the absence of profilin, from Fig. 2D, we estimate $k_{off}/k_{on} \approx 10$ nM. This ratio is the combination of k_{on} and k_{off} that is important in determining the polymerization curve since the probability p of a formin-associated filament to be bound to an oligomer, equal to the fractional decrease of elongation rate, is $p = 1/[1 + k_{off}/(k_{on} O_{\text{free}})]$.

With the above numbers for oligomer association/dissociation to/from formin-associated barbed ends, good fits to the data of Fig. 4 in the presence of formins and oligomers can be found by assuming that oligomers bind and inhibit free mDia1(14PP) formins with $K_{OF_{\text{free}}}^{d} = 0.8$ nM in the presence and $K_{OF_{\text{free}}}^{d} = 5$ nM in the absence of profilin (fig. S8D,E).

We further compared the model to the results of experiments with truncated FH1 domains (fig. S6), which is described in the model by parameter r_{PP}. In the absence of profilin, the mechanisms in the model do not predict any dependence of polymerization on r_{PP}. Parameters similar to those of fig. S8D can describe the curves in the absence of profilin in panels S6A,C,E. In the presence of profilin, fitting the data for mDia1(2PP) and mDia1(FH2) in fig. S6D,F requires a weaker inhibition of nucleation by oligomers as compared to mDia1(14PP): $K_{OF_{\text{free}}}^{d}$ has to be increased by one or two orders of magnitude. This result is consistent with the decreased inhibition of elongation for the same constructs in the presence of profilin (Fig. 3B). No significant change in the nucleation rate constants by formins was required for the

simulations of truncated mDia1, which is consistent with studies that found a relatively weak effect of the FH1 domain in nucleation in the presence of profilin (*34*).

Finally, the effect of weaker binding of pyrene-actin to profilin was also tested by: (i) including a higher dissociation constant for binding of pyrene-actin to profilin, and (ii) reducing the rate of FH1-mediated pyrene-actin polymerization (*11*). While simulated curves of polymerized pyrene-actin exhibited slower kinetics as compared to those of unlabeled actin, the conclusions regarding the effect of oligomers remained unchanged.

Figure S1

A

| Time, min: | 0 | 10 | 20 | 30 | 40 | 50 | 60 | 90 | 120 | 180 | 240 | Inactive ACD 240 |

Panel 1 — oligo, trimer, dimer, mono — 0.25 nM ACD

| | 0 | 15 | 30 | 45 | 60 | 90 | 120 | 180 | 240 | 240 |

Panel 4 — oligo, trimer, dimer, mono — 0.25 nM ACD

Panel 2 — oligo, trimer, dimer, mono — 1 nM ACD

Panel 5 — oligo, trimer, dimer, mono — 1 nM ACD

Panel 3 — oligo, trimer, dimer, mono — 1 nM ACD

Panel 6 — oligo, trimer, dimer, mono — 1 nM ACD

B

0.25 nM ACD — Crosslinked actin, % vs Time, min

1 nM ACD — Crosslinked actin, % vs Time, min

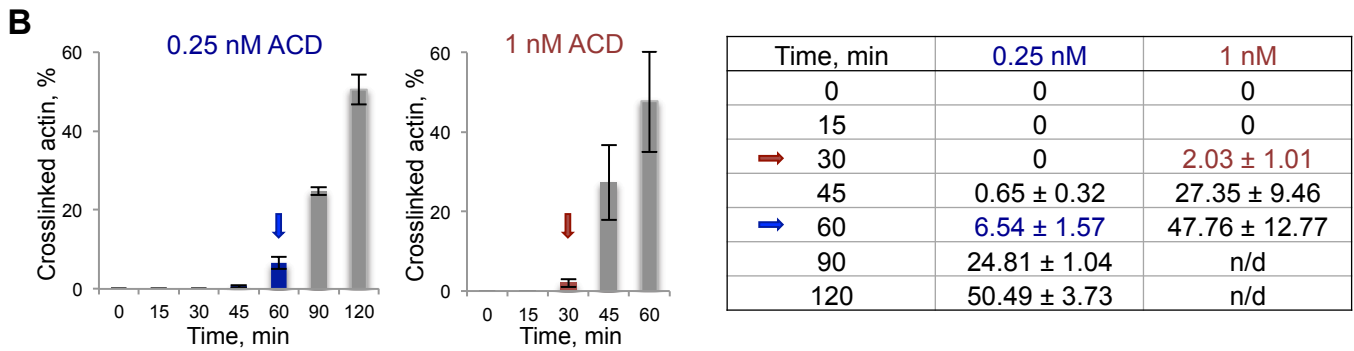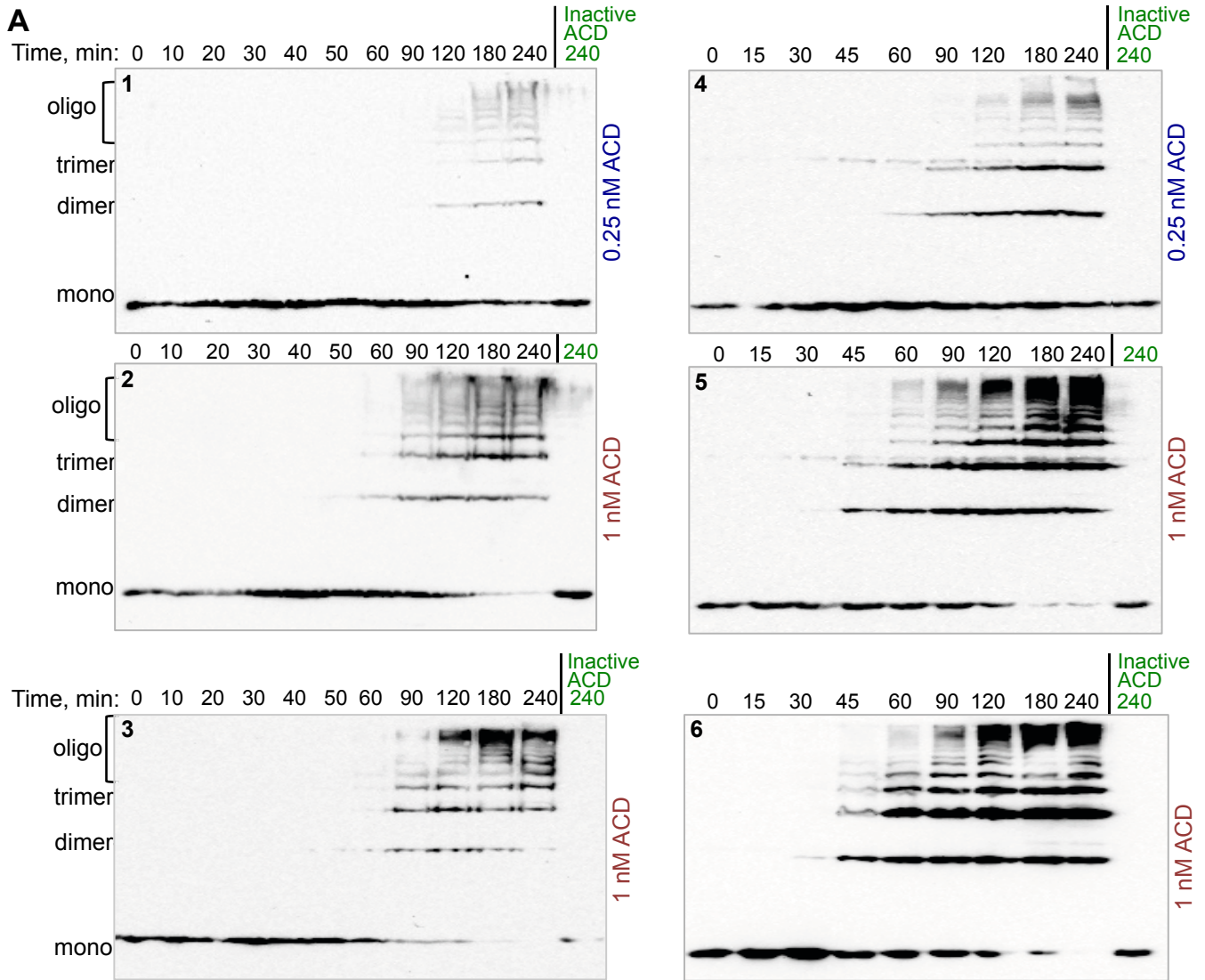| Time, min	0.25 nM	1 nM
0	0	0
15	0	0
→ 30	0	2.03 ± 1.01
45	0.65 ± 0.32	27.35 ± 9.46
→ 60	6.54 ± 1.57	47.76 ± 12.77
90	24.81 ± 1.04	n/d
120	50.49 ± 3.73	n/d

17

Fig. S1.

Quantitation of crosslinked actin in IEC-18 cell lysates upon LF$_N$ACD treatment.

(**A**) Anti-actin immunoblots of IEC-18 cells treated with 1 or 0.25 nM of LF$_N$ACD: blots #1-5 and the anti-actin blot on main Fig. 1D were stained with Thermo Scientific ACTN05 (C4) antibody; blot #6 and both blots on main Fig. 1B – with Sigma A2228 antibody. (**B**) Percent of crosslinked actin was quantified by densitometry. Data in graphs and table represent percent of crosslinked actin (mean ± SEM), number of experiments N=3 for 0.25 nM ACD and N=5 for 1 nM ACD treatment. Although only the lanes with low level of crosslinked material were quantified, the results must be interpreted with caution. Given that the net signal from the oligomers exceeds by many fold the signal from the uncrosslinked actin, the yield of actin crosslinking is likely to be overestimated. Arrows indicate the time points, at which the electrical resistance of epithelial monolayers dropped by ~50% (see main Fig. 1A) while only 2 – 6% of total actin was crosslinked into oligomers.
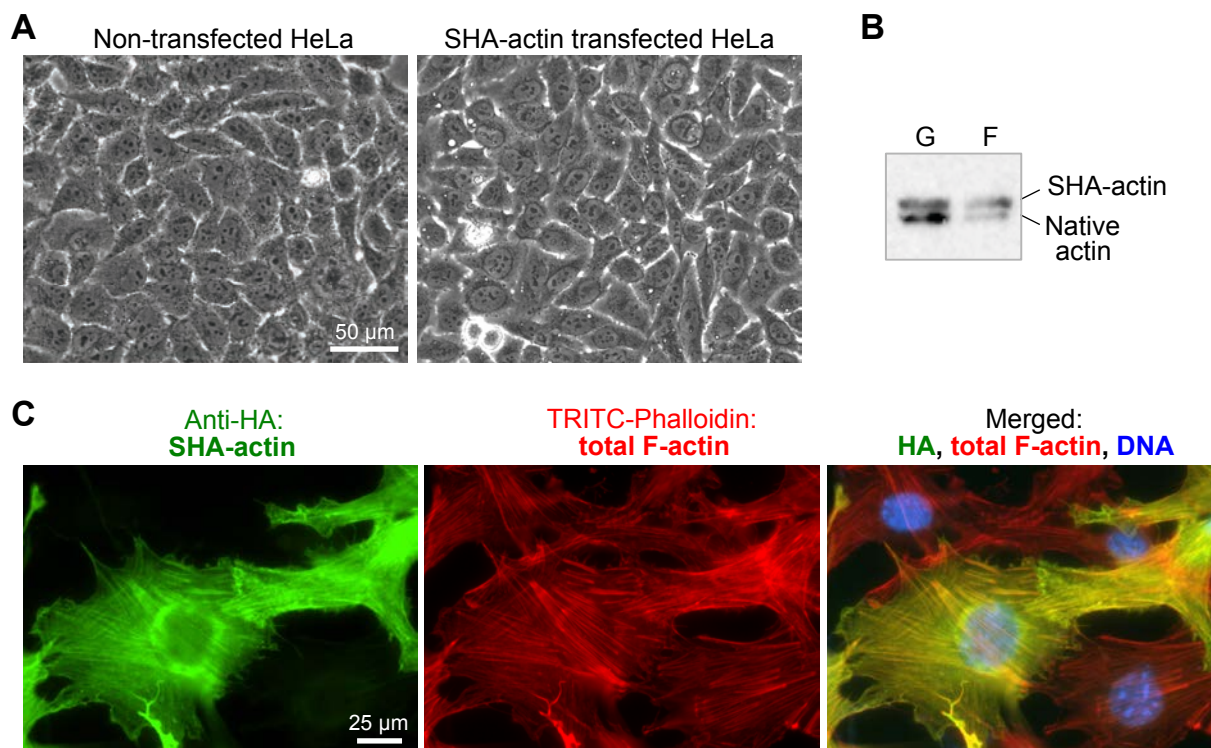
Figure S2

A   Non-transfected HeLa   SHA-actin transfected HeLa   **B**

C

Anti-HA:
SHA-actin

TRITC-Phalloidin:
total F-actin

Merged:
HA, **total F-actin**, **DNA**

Fig. S2

Actin double-tagged at the N-terminus with Twin-Strep-tagII and HA tags (SHA-actin) retained its polymerization abilities.

(**A**) HeLa cell morphology was unchanged following 24 h post-transfection with double-tagged (SHA) actin, compared to non-transfected cells. Scale bar is 50 μm. (**B**) Distribution of G- and F-actin in HeLa cells was similar for both native untagged and SHA-tagged actin as revealed by G- and F-actin fractionation and anti-actin immunoblotting. (**C**) 3T3 mouse fibroblasts were transfected with SHA-actin, stained with anti-HA antibody (SHA-actin, green), and counterstained with TRITC-phalloidin (total actin, green) and Hoechst (nucleic acid, blue). Scale bar is 25 μm. SHA-actin incorporated into stress fibers of 3T3 cells implying that the N-terminally introduced tags do not interfere with actin polymerization.

A

B
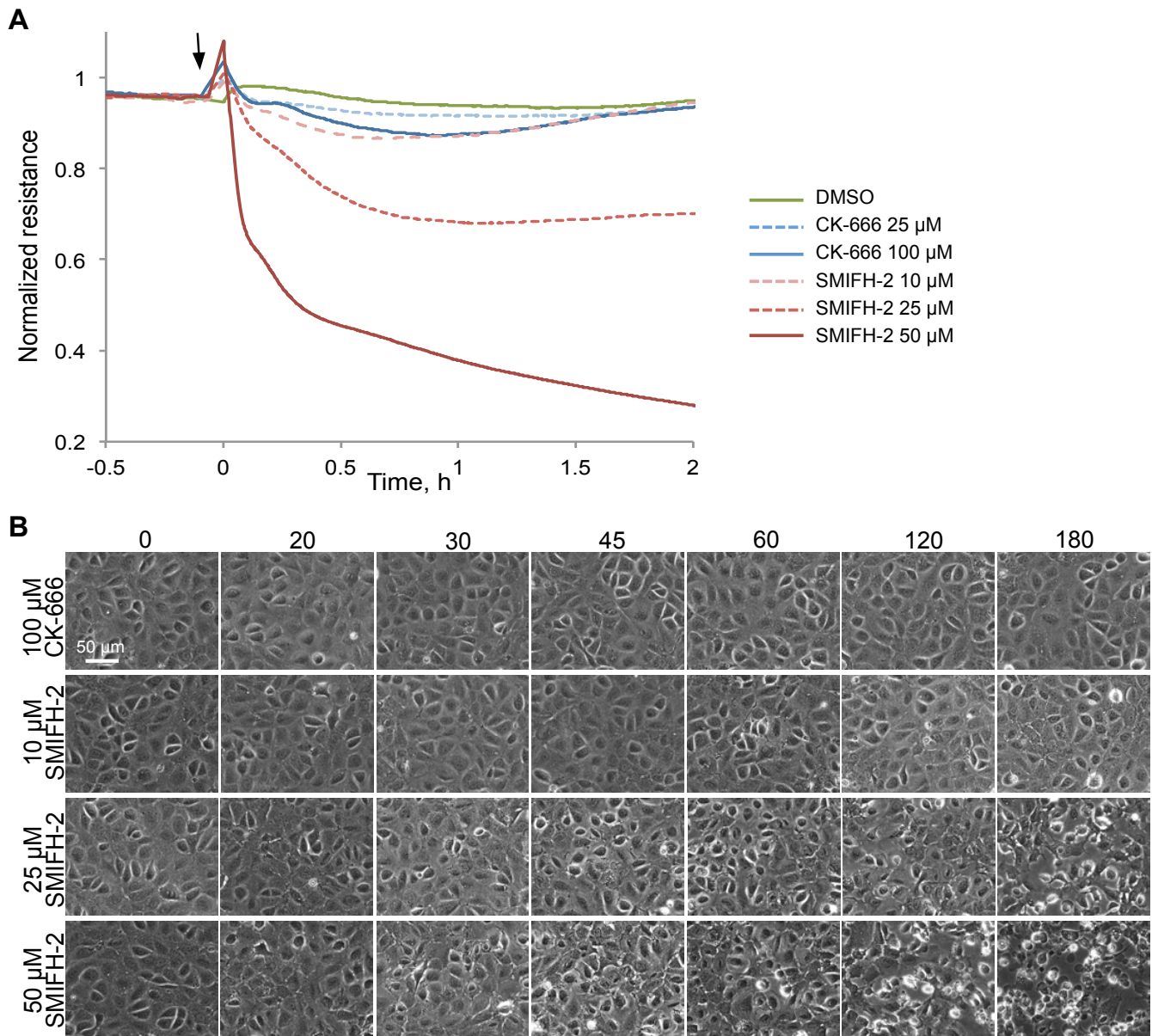
Fig. S3

Transepithelial electrical resistance (TEER) of intestinal monolayers was affected by formin inhibitor SMIFH-2, but not by Arp2/3 complex inhibitor CK-666.

Normalized electrical resistance (**A**) and micrographs of IEC-18 epithelial monolayers (**B**) treated with indicated concentrations of CK-666 or SMIFH-2. Scale bar is 50 μm. Arrow on (**A**) indicates addition of the inhibitors. Numbers above images on (**B**) indicate time in minutes.

Figure S4

A

Elongation rate, subunits/s

- Before stops
- After stops

[A-Olligo], nM: 0, 1, 3, 10

B Without PFN1

Actin subunits

mDia2-free

mDia2-controlled

Time, s

Flow 20 nM A-Oligo

C With PFN1

Actin subunits

mDia2-controlled

mDia2-free

Time, s

Flow 20 nM A-Oligo

D 1 nM mDia1(FH2) / without PFN1

0 nM Oligomers 100 nM Oligomers

5 µm 5 µm

E 1 nM mDia1(FH2) / without PFN1

Number of filaments

- 0 nM Oligomers
- 100 nM Oligomers

*

F 10 nM mDia1(FH2) / with PFN1

0 nM Oligomers 150 nM Oligomers

5 µm 5 µm

G 10 nM mDia1(FH2) / with PFN1

Number of filaments
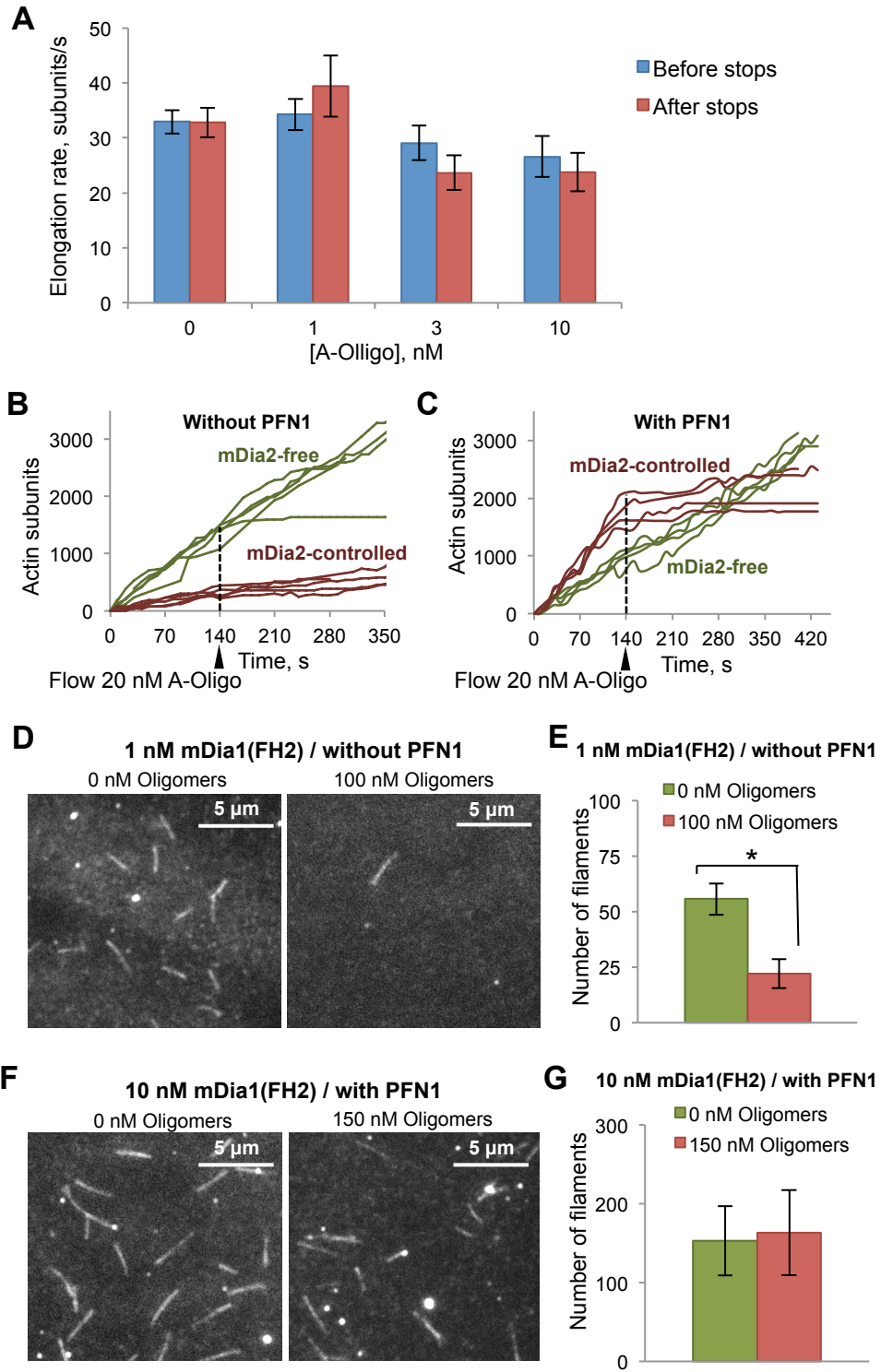
- 0 nM Oligomers
- 150 nM Oligomers

Fig. S4

Effects of ACD-crosslinked actin oligomers on formin-mediated actin polymerization in TIRFM.

(**A**) Elongation rates of mDia1(14PP)-controlled actin filaments in the presence of PFN1 measured before and after elongation pauses caused by the presence of oligomers. Error bars represent SEM, $N>10$. (**B**, **C**) Plots of SNAP-mDia2-controlled (10 nM formin, 1.5 µM actin) and free filament elongation before and after the flow of 20 nM actin oligomers (indicated by arrowhead) in the absence (**B**) and in the presence (**C**) of 2.5 µM PFN1. (**D-G**) In the presence of actin oligomers, nucleation by mDia1(FH2) was decreased in the absence of PFN1 (**D**, **F**), but not the in presence of PFN1 (**E**, **G**) as measured by counting the total number of filaments in the field (5450 µm^2) 3 min after the initiation of polymerization. Error bars in **E** and **G** represent SEM, N=3; * - p<0.05 determined by Student's t-test. TIRF images (**D** and **F**) were taken 3 min post-flow; areas smaller than those used for analysis are shown.
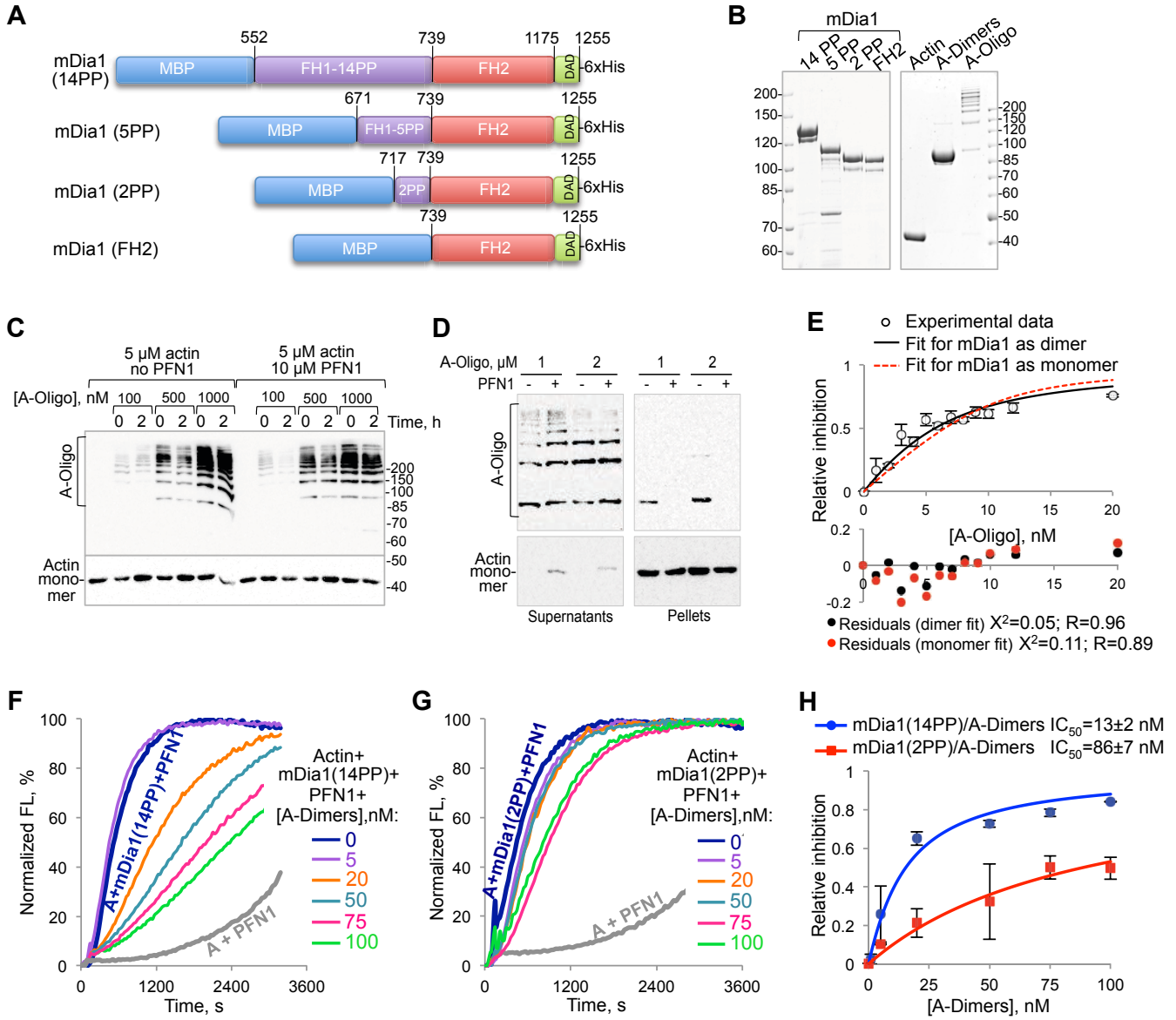
Figure S5

Fig. S5

ACD-crosslinked actin species dose-dependently inhibited actin polymerization directed by mDia1 in bulk pyrenyl-actin polymerization assays.

(**A**) Schematic representation of mDia1 constructs. MBP – maltose binding protein tag; FH1 – formin homology 1 domain containing different number of polyproline regions (14PP, 5PP, and 2PP – are FH1 with 14, 5, and 2 polyproline regions, correspondingly); FH2 – formin homology 2 domain; DAD – diaphanous autoregulatory domain; 6xHis – hexa-histidine-tag. Numbers correspond to residue numbers in mDia1 (NCBI accession number NP_031884.1). (**B**) SDS-PAGE of representative mDia1 constructs and actin species used in the present studies. A-Dimers and A-Oligo – ACD-crosslinked actin dimers and oligomers, respectively. (**C**) Anti-actin immunoblot showed no accumulation of additional crosslinked actin species after 2 h incubation of oligomers with actin in the pyrene-actin assay buffer even when high oligomer concentrations are used, confirming the complete inhibition of ACD activity in the actin oligomer preparation. (**D**) Actin (10 μM) and crosslinked actin oligomers (1 and 2 μM) were allowed to polymerize in the presence or absence of PFN1 and subjected to ultracentrifugation (300,000 g) to separate filamentous (pellet) and non-polymerized (supernatant) actin, which were probed by anti-actin immunoblotting. Note, that the majority of oligomeric actin species did not polymerize and stayed in the supernatant fractions. In the absence of PFN1, some incorporation of the crosslinked actin species into actin filaments (pellet fractions) occurred, tentatively explaining elevated polymerization rates observed at high concentrations of the oligomers (Fig. 4A). (**E**) The inhibition of mDia1(14PP)-mediated actin polymerization by the oligomers was fitted to the binding isotherm equation considering formin as a dimer (black) or as a monomer (red). Plot of residuals and fitting parameters for both fits are shown below the graph. (**F**, **G**) Effects of isolated ACD-crosslinked actin dimers (A-Dimers) on actin polymerization mediated by 5 nM of mDia1(14PP) (**F**) and mDia1(2PP) (**G**) in the presence of PFN1. (**H**) Inhibition of formin-mediated filament growth by ACD-crosslinked actin dimers in the presence of PFN1. Error bars represent SEM.

Figure S6
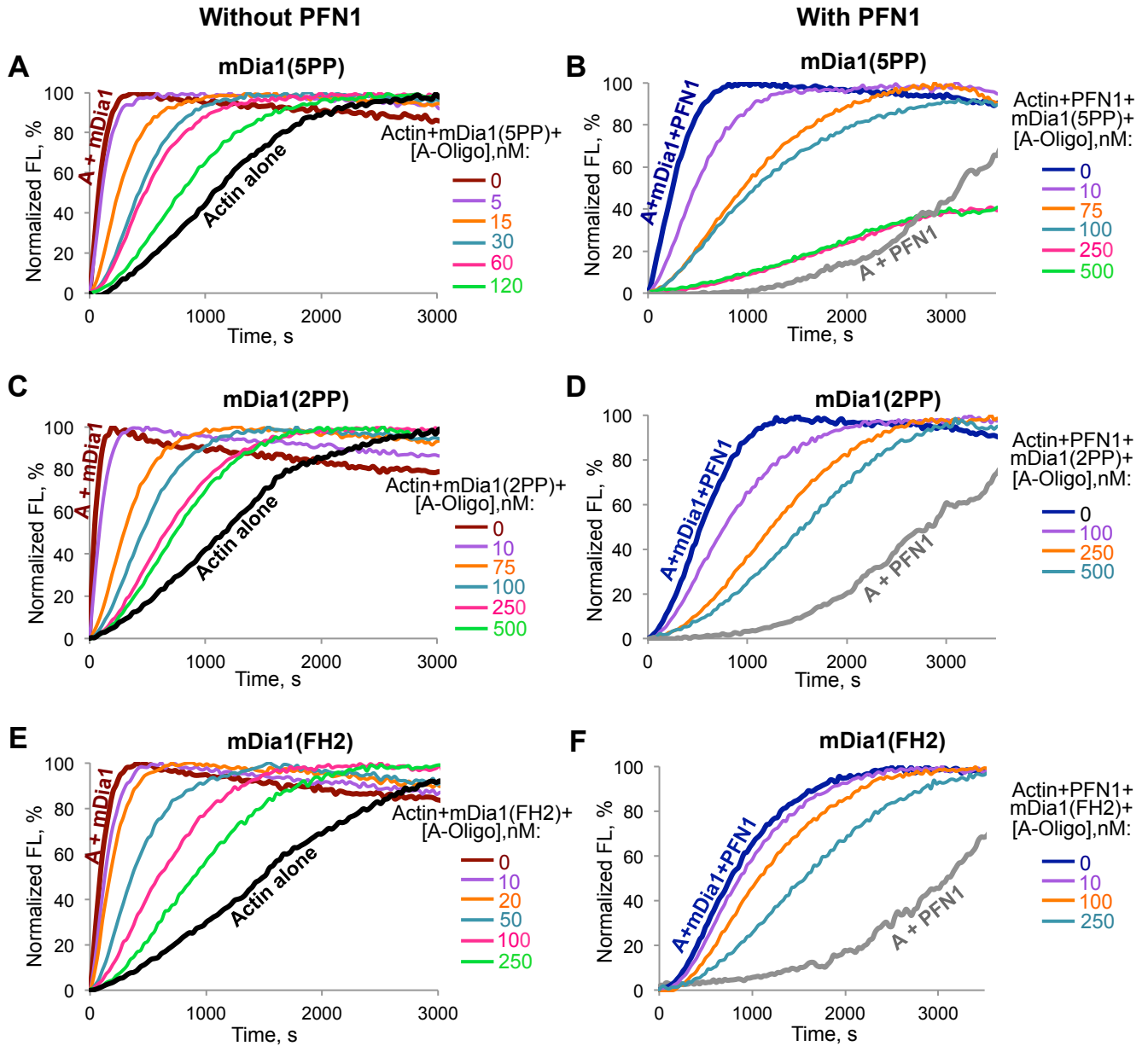
Fig. S6

Effects of oligomers on actin polymerization mediated by mDia1 constructs with truncated FH1 domain.

Effects of various oligomer concentrations on polymerization of 2.5 µM actin mediated by 10 nM of mDia1 constructs with truncated FH1 domain in the absence of PFN1 (**A, C, E**) or in the presence of 5 µM PFN1 (**B, D, F**). (**A, B**) mDia1(5PP). (**C, D**) mDia1(2PP). (**E, F**) mDia1(FH2). The effects were quantified and the results are presented on Fig. 4E,F.

Figure S7

A

Fluorescence, au

Actin+seeds:[Actin+mDia1(14PP)]
Actin (no seeds)
Actin+seeds:
[Actin+
mDia1(14PP)+
100nM A-Oligo]

Time, s

B

Fluorescence, au

Actin+PFN1+seeds:[Actin+mDia1(14PP)]
Actin+PFN1 (no seeds)
Actin+PFN1+seeds:
[Actin+
mDia1(14PP)+
100nM A-Oligo]

Time, s

C

Fluorescence, au

Actin+seeds:[Actin+mDia1(FH2)]
Actin (no seeds)
Actin+seeds:
[Actin+
mDia1(FH2)+
100nM A-Oligo]

Time, s

D

Fluorescence, au

Actin+PFN1+seeds:[Actin+mDia1(FH2)]
Actin+PFN1
(no seeds)
Actin+PFN1+seeds:
[Actin+
mDia1(FH2)+
100nM A-Oligo]

Time, s

E

PFN1-free mDia1(14PP) seeds

Barbed ends, fmol

Actin
Actin+PFN1
(PFN1 added
after seeding)

no seeds
[mDia1(14PP)] seeds
[mDia1(14PP)+ A-Oligo] seeds

F

PFN1-free mDia1(FH2) seeds

Barbed ends, fmol

Actin
Actin+PFN1
(PFN1 added
after seeding)

no seeds
[mDia1(FH2)] seeds
[mDia1(FH2)+ A-Oligo] seeds

G

Fluorescence, au

Actin+seeds:[Actin+mDia1(FH2)]
Actin+seeds:
[Actin+
mDia1(FH2)+
A-Oligo+PFN1]
PFN1+mDia1(FH2)]
Actin (no seeds)

Time, s

H

Fluorescence, au

Actin+PFN1+seeds:
[Actin+PFN+mDia1(FH2)]
Actin+PFN1+seeds:
[Actin+
mDia1(FH2)+
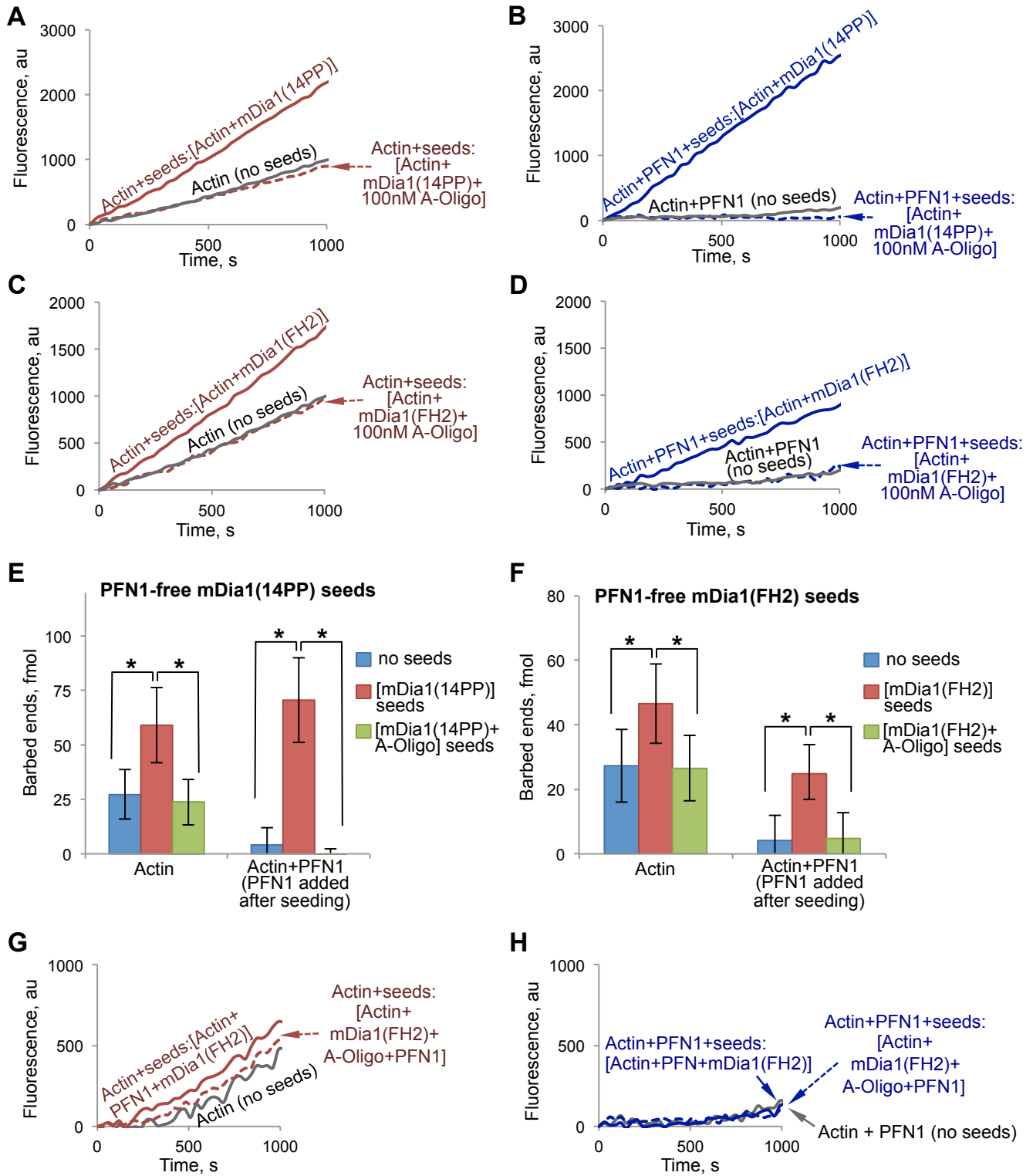A-Oligo+PFN1]
Actin + PFN1 (no seeds)

Time, s

26

Fig. S7

Pyrenyl-actin polymerization seeding assays.

(**A-D**) Effects of actin oligomers (A-Oligos) on filament nucleation by mDia1(14PP) or mDia1(FH2). Seeds were generated by incubation of 2.5 μM of unlabeled actin in the absence of PFN1 with 10 nM mDia1(14PP) (**A, B**) or mDia1(FH2) (**C, D**) for 1.5 min in the presence or absence of oligomers, after which point they were diluted 100-fold and used as templates for elongation of 1 μM of 5% pyrenyl-actin in the absence (**A**, **C**) or presence of 5 μM PFN1 (**B**, **D**). Note that PFN1 in this case was used to inhibit spontaneous nucleation at the elongation stage, and not during the seeding stage of the experiment. (**E**, **F**) Quantitation of barbed ends formed was determined from the slope of each line. Error bars represent SEM, *N*=3; * - p<0.05 determined by Student's t-test. (**G**, **H**) Effects of the oligomers on formin-controlled nucleation in the presence of PFN1 were evaluated in a similar way except that only mDia1(FH2) was used and seeds for elongation of 1 μM of 5% pyrenyl-actin in the absence (**G**) or presence of 5 μM PFN1 (**H**) were extracted after 5 min after initiation of polymerization in the presence of PFN1. "au" – arbitrary units.
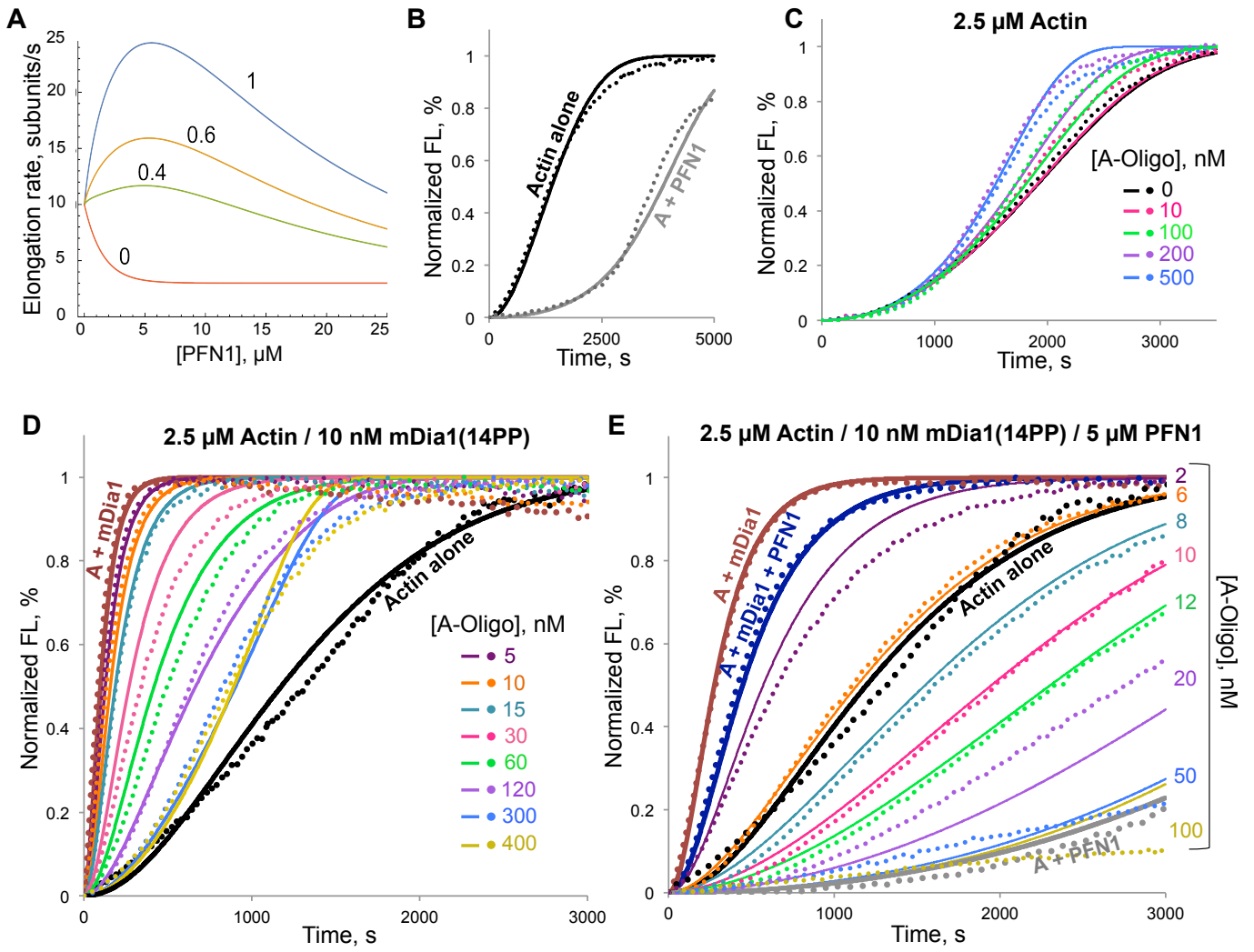
Figure S8

Fig. S8

Modeling of actin filament nucleation and elongation in the presence of ACD-crosslinked actin oligomers. (Detailed explanations are given in the model description.)

(**A**) Plot of elongation rate in subunits per second as a function of total PFN1 concentration at 1 μM of total actin using Equation (3). r_{PP} values reflect the reduction of FH1-mediated polymerization for formin constructs with truncated FH1 domains. (**B-E**) Modeled (solid lines) versus experimental data (dotted lines) graphs of the effects of actin oligomers (A-Oligo) on actin polymerization in the absence (**B**, **C**) or presence of mDia1(14PP) (**D**, **E**); without (**C**, **D**) or with PFN1 (**E**). Experimental data in C, D, and E correspond to the experimental data shown on Fig. 4A, C, and D, respectively. Model and experimental curves for actin alone (black) in (**E**) are the same as in (**D**). The parameter values used for the modeling are shown in Table S1.

A

Actin State			
Multiple binding sites	No	Yes	Yes
G-actin binding proteins (e.g. profilin)	Bind	Not	Bind

Actin subunit (G-actin)   Profilin   F-actin

ACD-crosslinked actin oligomers

FH1   Formin   FH2

B

Profilin-dependent inhibition
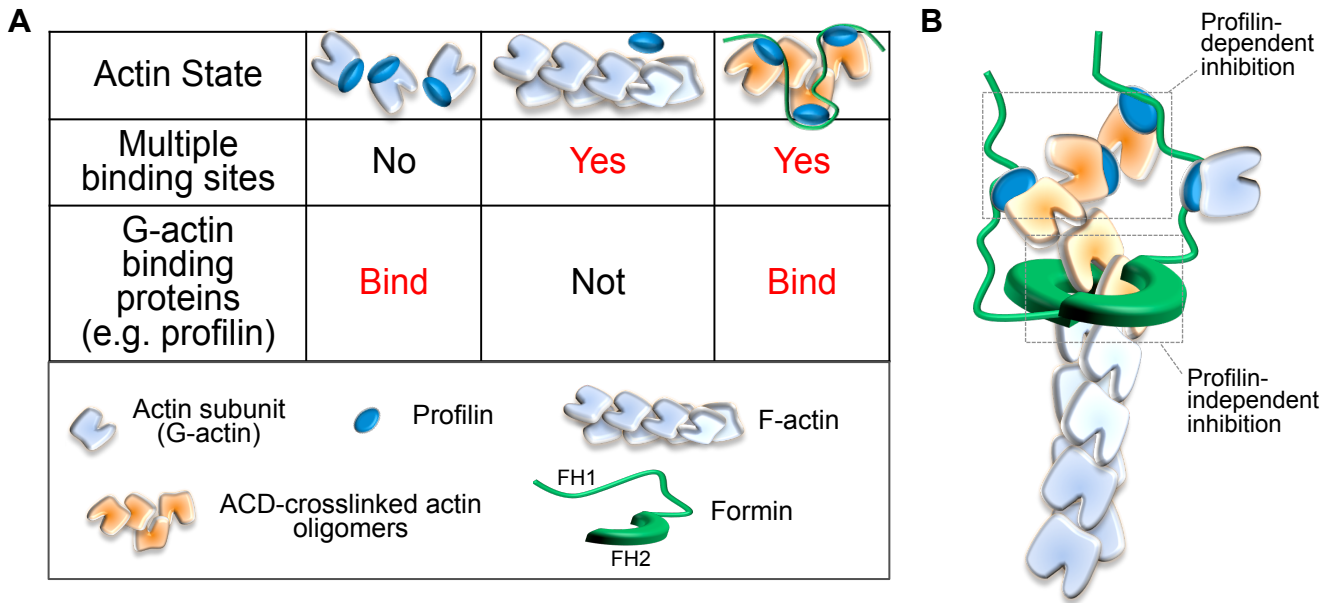
Profilin-independent inhibition

Fig. S9

Mechanism of formin inhibition by ACD-crosslinked actin oligomers.

(**A**) In contrast to both G- and F-actin, the ACD-crosslinked oligomers can bind with abnormally high affinity to proteins with multiple G-actin binding sites (e.g. formins). (**B**) The oligomers potently block formin-mediated actin polymerization in profilin-dependent and independent modes. Because the cellular concentration of formins is orders of magnitude lower than that of actin, the toxicity develops faster and under lower doses of the toxin.

Table S1. Model parameter values.

	fig. S8B	fig. S8C	fig. S8D	fig. S8E
k_A^+ (μM^{-1}s^{-1})	10	10	10	10
k_A^{nuc} (μM^{-2}s^{-1})	$5 \cdot 10^{-9}$	$1.8 \cdot 10^{-9}$	$8 \cdot 10^{-9}$	$8 \cdot 10^{-9}$
k^{frag} (s^{-1})	$5 \cdot 10^{-8}$	$7 \cdot 10^{-8}$	$3 \cdot 10^{-8}$	$2 \cdot 10^{-8}$
K_{PA}^d (μM)	0.7			0.7
k_{PA}^+ (μM^{-1}s^{-1})	10			10
k_O^+ (μM^{-1}s^{-1})		0.02 [a]	0.02 [a]	0.0045 [a]
k_O^{sev} (s^{-1})		$3 \cdot 10^{-3}$ [a]	10^{-3} [a]	$4 \cdot 10^{-4}$ [a]
k_{AF}^{nuc} (μM^{-2}s^{-1})			$6 \cdot 10^{-4}$	$7 \cdot 10^{-5}$
k_{APF}^{nuc} (μM^{-2}s^{-1})				$6 \cdot 10^{-5}$
k_{on} (μM^{-1}s^{-1})			0.5 [b]	2.8
k_{off} (s^{-1})			0.05 [b]	0.007
$K_{OF_{free}}^d$ (nM)			5	0.8

[a] The value of the product $k_O^+ k_O^{sev}$ is relevant in simulations.

[b] The value of the ratio k_{off} / k_{on} is relevant in simulations.

Captions for Movies

Movie S1

Polymerization of individual actin filaments by evanescent wave microscopy in the absence of ACD-crosslinked actin oligomers.

Polymerization of Oregon green (OG) actin (1.5 µM, 33% labeled) mediated by 5 nM of mDia1(14PP) from profilin-actin (1.7:1) complexes was monitored in the absence of oligomers. Green arrowheads denote selected mDia1-controlled (dim and fast) barbed ends; yellow arrowheads point to mDia1-free (bright and slow) barbed ends. Movie S1 is related to Fig. 2A (top panel).

Movie S2

Polymerization of individual actin filaments by evanescent wave microscopy in the presence of ACD-crosslinked actin oligomers.

OG-actin (1.5 µM, 33% labeled) polymerization mediated by 5 nM of mDia1(14PP) from profilin-actin complexes was monitored in the presence of 1 nM oligomers. Green and yellow arrowheads are as in Movie S1; red arrowheads point to mDia1-controlled barbed ends stopped by the oligomers. Movie S2 is related to Fig. 2A (bottom panel).

Movie S3

Effects of ACD-crosslinked actin oligomers on polymerization of individual filaments by evanescent wave microscopy.

Polymerization of OG-actin (1.5 µM, 20% labeled) was monitored in the presence of 10 nM of mDia1(14PP) and profilin (1.7:1 ratio to actin) in the absence of oligomers. Green arrowheads point to mDia1-free (bright and slow) barbed ends; red arrowheads point to mDia1-controlled (dim and fast) barbed ends. As indicated, a mixture of OG-actin (1.5 µM, 40% labeled), profilin (2.5 µM) and oligomers (20 nM)

was flowed into the chamber. Note paused mDia1-controlled (red arrowheads), but not mDia1-free (green arrowheads), filaments after the flow of oligomers.

Movie S4

Dual-color TIRFM.

TMR-labeled (red) actin (1.5 μM, 15% labeled) was polymerized in the presence of 5 nM mDia1 and 2.5 μM profilin without actin oligomers for 200 sec and then the working chamber solution was replaced with OG-actin (1.5 μM, 33% labeled), actin oligomers (20 nM), and profilin (2.5 μM). Arrowheads are as in Movies S1 and S2. Movie S4 is related to Fig. 2E.

Movie S5

Effects of ACD-crosslinked actin oligomers on polymerization of individual filaments mediated by SNAP-549-mDia2.

OG-actin (1.5 μM, 20% labeled) polymerization in the presence of SNAP-549-mDia2 (10 nM) and profilin (2.5 μM) was monitored for 2 min 45 sec followed by a flow of a mixture of OG-actin (1.5 μM, 40% labeled), profilin (2.5 μM), and oligomers (20 nM). Red arrowhead indicates SNAP-549-mDia2 (red dot) attached to an actin filament; white arrowhead indicates formin-independent filament. Note a pause of mDia2-controlled filament with the attached SNAP-549-mDia2, but not formin-free filament, upon oligomer flow. Movie S5 is related to Fig. 3A.